Progress in Natural Science: Materials International 27 (2017) 93–98

Contents lists available at ScienceDirect

Progress in Natural Science: Materials International

journal homepage: www.elsevier.com/locate/pnsmi

Original Research

Effect of nanoparticle (Pd, Pd/Pt, Ni) deposition on high temperature hydrogenation of Ti-V alloys in gaseous flow containing CO

S. Suwarno[a,d,*], M. Williams[b, c], J.K. Solberg[d], V.A. Yartys[b,d]

[a] Department of Mechanical Engineering, Institut Teknologi Sepuluh Nopember, Surabaya, 60111, Indonesia
[b] Institute for Energy Technology, P.O. Box 40, NO-2027, Kjeller, Norway
[c] University of the Western Cape, Private Bag X17, Bellville 7535, South Africa
[d] Department of Materials Science and Engineering, NTNU, NO-7491, Trondheim, Norway

ARTICLE INFO

Keywords:
Metal hydride
Titanium
Vanadium
Nanoparticle
Palladium
Nickel
Platinum
Carbon monoxide

ABSTRACT

The hydrogenation properties of Ti-V hydrides coated with nanoparticles have been studied in gaseous mixtures of argon and hydrogen with and without additions of 1% CO. Nanoparticles of Pd, Ni, and co-deposited Pd/Pt with particle sizes of ~30–60 nm were formed by electroless deposition on the hydride surfaces. The alloy resistance to CO could be significantly improved by particle deposition. Large amounts of hydrogen were absorbed in a CO-containing gas when Ni and Pd/Pt deposition had been applied, while pure Pd deposition had no positive effect. Ni was found to have a stronger effect than those of Pd/Pt and Pd, possibly because of the size effect of Ni nanoparticles.

1. Introduction

Industrial hydrogen can be produced from different sources using various production methods. Large scale hydrogen production is conventionally carried out by steam reforming of hydrocarbons. The hydrogen sorption enhanced reforming (HSER) [1] is a recently proposed concept aiming to increase the efficiency of conventional steam reforming by using a metal/alloy as an in situ hydrogen absorbent. Thermodynamic modeling has shown that HSER has a potential for increased energy efficiency and reduced operation temperatures of steam reforming. However, HSER faces challenges in its realization since the process gas contains significant amounts of active gases as CO and H_2O, which inhibits the hydrogen-metal interaction. For hydrogen storage alloys, CO was found to be the strongest contributor to their deactivation. It has been suggested that chemisorption on the alloy surface leads to blocking of hydrogen-active sites, thus decreasing the reactivity of the alloy towards hydrogen [2–4].

Another requirement for HSER applications is that the hydride must form and decompose at high temperatures, i.e. 400–800 °C, where most metal hydrides become unsuitable. Because of their thermodynamic stability, Ti-V based hydrides have been investigated as promising candidates for hydrogen absorption in HSER application [5]. These alloys were selected due to the high thermal stability of their hydrides and high volumetric hydrogen density. Our previous study [5] showed that the hydrogen absorption kinetics was excellent, and the alloys absorbed up to 3.96 wt% H at room temperature within less than 60 s and up to 3.5 wt% H at 450 °C within 5 min. However, the sorption capacity of the alloy was pronouncely degraded when the cycling was performed in flows of hydrogen and active gases as CO.

Electroless deposition of metals can improve hydrogenation kinetics and the tolerance towards active gases at low concentrations. [6]. Williams et al. reported easy activation of AB_5 alloys after electroless Pd deposition [7,8] of particles down to 63 nm in average size. A similar positive result has been reported for Ti-Fe based alloys [9].

Our previous work showed that Ti-V alloys were able to absorb limited amounts of hydrogen when CO was present in the gaseous flow [10]. In the present work, the effect of deposition of Ni-, Pd- and co-deposited Pd/Pt nanoparticles on hydrogen absorption and desorption of Ti-V is studied in detail.

2. Materials and experimental methods

2.1. Sample preparation and nanoparticle deposition

$Ti_{0.9}V_{0.1}H_2$ was prepared by hydrogenation of an arc-melted button following the procedures described in a previous paper [11]. During

Peer review under responsibility of Chinese Materials Research Society.
* Corresponding author.
E-mail address: warno@me.its.ac.id (S. Suwarno).

http://dx.doi.org/10.1016/j.pnsc.2017.01.003
Received 18 October 2016; Accepted 30 November 2016
Available online 04 February 2017

hydrogenation, millimeter-size particles were pulverized to hydride powder particles being less than 200 μm in size. The nanoparticle deposition was performed by an electroless method. The details of the method to deposit nanoparticles on the hydride surface have been given by Williams et al. [6–8]. In short, the method includes the following three main steps (1) The powder surface is activated by using a colloidal solution containing Pd and Sn so that pure Pd nucleates at the hydride particle surface; (2) Sn which was deposited in step (1) was later removed from the powder by suspending it into a Na_2EDTA reducing solution; (3) Deposition of Pd onto the powder surface by immersion into an electroless plating bath containing $PdCl_2$ and a reducing agent, NH_4OH. Deposition of Pd/Pt particles was conducted by sequential deposition, i.e. an additional step was added for Pt deposition after the Pd deposition was completed. This was done by immersion of the Pd deposited hydride powder into a Pt electroless plating bath consisting of a solution of $Na_2Pt(OH)_6$ containing a reducing agent. Ni followed a procedure similar to Pd deposition except that a different reducing agent was used, i.e. sodium hypophosphate (NaH_2PO_2).

Hydrogen absorption and desorption in a gaseous flow were performed in a temperature-programmed reduction (TPR) apparatus connected to a mass spectrometer (MS) from Pfeiffer Vacuum GmbH. The MS was calibrated to determine concentrations of H_2, Ar, CH_4, CO, CO_2, O_2 and H_2O in the outgoing flow. The concentration vs. time profiles were then plotted and gave the amount of hydrogen absorbed and desorbed during the measurements.

Laboratory scale XRD was performed using a Bruker D8 Focus with a Cu Kα X-ray source. A powder sample was dispersed in the silicon sample holder using ethanol as a dispersing agent. Powder diffraction patterns were collected using a squared slit with 0.6 mm side length. The data was typically collected with 2θ steps of 0.01 deg from 10 deg to 90 while the sample holder was rotated regularly. A Zeiss Ultra 55LE field emission scanning electron microscope (FE-SEM) equipped with an EDS detector was used to examine the powder. For this purpose, a small quantity of powder was dispersed on a carbon tape attached to the SEM sample holder. The surface morphology of the powder was investigated in secondary electron mode applying 5 kV accelerating voltage.

3. Results and discussion

3.1. Sample morphology

A hydride surface containing electroless deposited nanoparticles is shown in Fig. 1. As can be seen in Fig. 1a, Pd/Pt nanoparticles were finely dispersed on the hydride surface. Individual nanoparticles had spherical shape and were in average about 60 nm in size. Nanoparticles of only Pd (not shown) had approximately the same size and distribution as those of Pd/Pt. The surface morphology of sample deposited with Ni nanoparticles is shown in Fig. 1b. A smaller average particle size is observed in this figure compared to in Fig. 1a, i.e. ~30 nm.

3.2. Hydrogenation and dehydrogenation properties

Hydrogen sorption studies on the $Ti_{0.9}V_{0.1}$ alloy in a mixture Ar+H_2 flow have been reported earlier [10]. The hydrogen desorption spectra obtained during TPR depend on the type of hydrides formed during the hydrogenation steps. Fig. 2 shows hydrogen desorption spectra from hydrides hydrogenated at various isothermal temperatures. An initially fully hydrogenated sample desorbed about 3.8 wt% H (named as des 1). Hydrogenation at high temperatures resulted in hydrides with lower hydrogen content. The dehydrogenation spectra contain a main peak at higher temperatures which corresponds to BCC β hydride dehydrogenation. The amount of desorbed hydrogen was 2.75, 2.39, 2.03 and 0.98 wt% for the samples hydrogenated at 425 °C, 475 °C, 525 °C, and 575 °C, respectively. Another important characteristic of the hydrogen

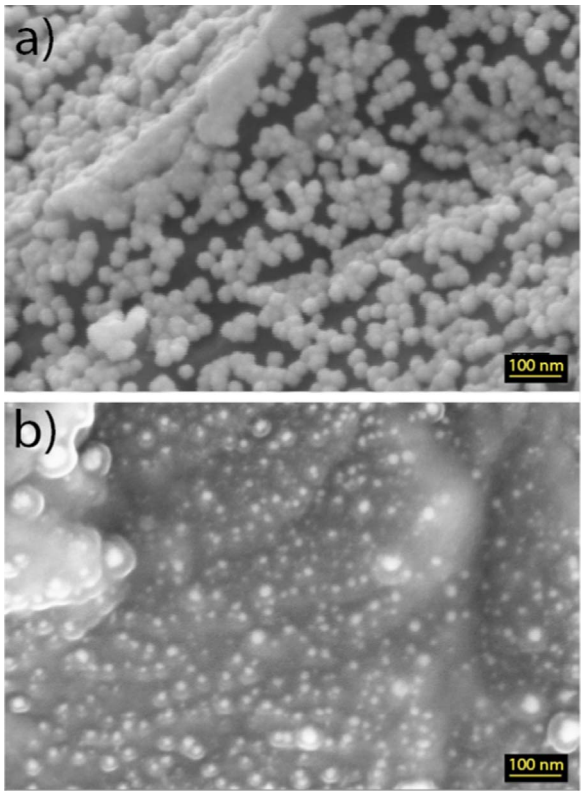

Fig. 1. Surface morphology of metal hydride surfaces with nanoparticle deposition: a) $Ti_{0.9}V_{0.1}H_2$+nano Pd/Pt, b) $Ti_{0.9}V_{0.1}H_2$+nano Ni.

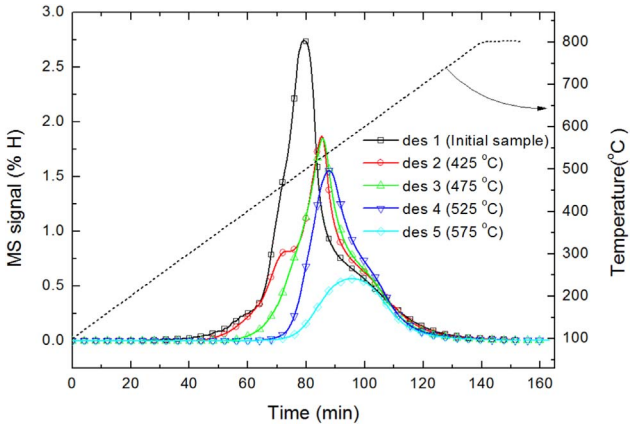

Fig. 2. Hydrogen desorption spectra of $Ti_{0.9}V_{0.1}H_X$ during heating from RT to 800 °C at 5 K/min heating rate in Ar flow. Desorption was done after hydrogenation in Ar+10%H_2 at isothermal temperatures given in the parentheses.

desorption spectra is shown in Fig. 2 and comprises the onset temperature of hydrogen desorption. It can be observed that it is related to the hydrogenation temperature. This shows that the hydrogen desorption from the formed hydrides, except for the 2nd desorption, depended on the thermal stability of the hydrides, which is very much affected by reactions at interfaces, rather than by the diffusion of hydrogen.

The effect of nanoparticle deposition on the $Ti_{0.9}V_{0.1}$ hydrogen sorption properties was also studied by performing TPR experiments. Seven TPR cycles were performed for each sample in different gaseous mixtures. The 1st cycle was desorption of a fully hydrogenated initial sample, from which 3.7–3.8 wt% hydrogen were desorbed. In the next 3 cycles (cycle 2–4), hydrogenation was done in Ar+H_2+1%CO at various isothermal temperatures, i.e. cycle 2: 425 °C, cycle 3: 475 °C and cycle 4: 525 °C. Dehydrogenation was always done non-isother-

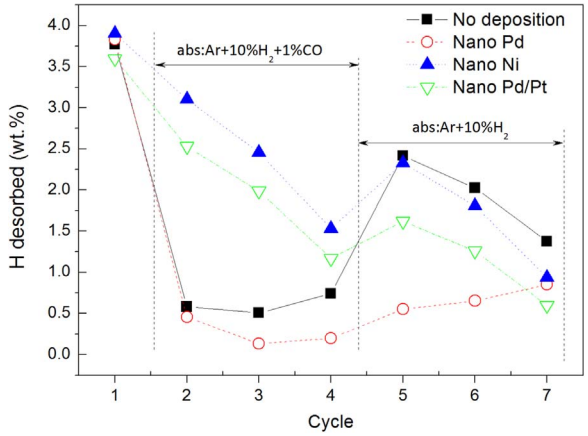

Fig. 3. Amount of hydrogen desorbed from the hydrides hydrogenated at various temperatures. Cycle 1: hydrogen desorbed from initial dihydride sample. Cycle 2–4: hydrogen absorption in 100 ml/min Ar+10%H_2+1%CO, desorption in 100% Ar. Cycle 5–7: hydrogen absorption in 50 ml/min Ar+10%H_2, desorption in 100% Ar. Hydrogenation was done isothermally at 425 °C (cycle 2, 4), 475 °C (cycle 3, 6), and 525 °C (cycle 4,7).

mally by heating the formed hydrides from 100 °C to 800 °C at 5 deg/min heating rate in Argon flow. During the last 3 cycles, cycle 5–7, the hydrogenation was done in Ar+H_2 at the same temperatures as used in cycles 2–4, i.e. 425 °C, 475 °C and 525 °C. The amounts of desorbed hydrogen were calculated from the hydrogen desorption spectra given in Fig. 3. It can be observed from this figure that non-catalyzed $Ti_{0.9}V_{0.1}$ absorbed only limited amounts of hydrogen, less than 0.5 wt% during the cycles 2–4. Indeed, the samples with deposited Ni and Pd/Pt absorbed much larger amounts of hydrogen when the hydrogenation was done in Ar+H_2. Ni was observed to have the best effect as can be seen from the figure. When it comes to the Pd nanoparticles without Pt, it can be seen from Fig. 3 that they did not improve the tolerance of the alloy towards CO.

In the subsequent cycles (cycle 5–7), CO was removed from the gas mixture flow. As can be seen from Fig. 3, this resulted in increased hydrogen desorption, e.g. the non-deposited sample recovered and absorbed ~2.5 wt% H during cycle 5, which is higher than the desorption from the nanoparticle-deposited samples.

The hydrogenation curves of non-deposited $Ti_{0.9}V_{0.1}$ recorded during cycle 5–7, i.e. hydrogenation at 425 °C, 475 °C and 525 °C, are shown in Fig. 4. From Fig. 4a it can be seen that some incubation time was required before hydrogen could be absorbed. The incubation time was shorter at higher temperatures. The incubation time is normally related to the time required for hydrogen to penetrate an oxide layer [12,13], and it is shorter at high temperatures because the diffusion coefficient increases with temperature. Surface microanalysis of the Ti-V alloys showed that the outer layer of the alloy surface was rich in oxygen [10]. Thus, the incubation time observed in Fig. 4a was probably caused by oxygen enrichment of the sample surface originating from interaction with CO during early cycling.

Fig. 4b shows hydrogenation curves of Pd/Pt nanoparticle-deposited $Ti_{0.9}V_{0.1}$. It can be seen that the hydrogen was absorbed without any incubation time. This means that Pd/Pt nanoparticles played a significant role and acted as hydrogen absorption paths. However, an increase in the hydrogenation temperature gave only a marginal improvement of the hydrogenation kinetics. The curves have other profiles than the curves obtained from the non-deposited samples, which indicates that the kinetics rate-limiting steps for the hydrogenation might be different.

Fig. 5 gives a comparison of the hydrogen absorption curves recorded at 475 °C for the samples with different surface deposition. As can be seen, the incubation time was relatively short or negligible for the two nanoparticle-deposited samples. The non-deposited sample needed approximately 8 min before hydrogen absorption started. The

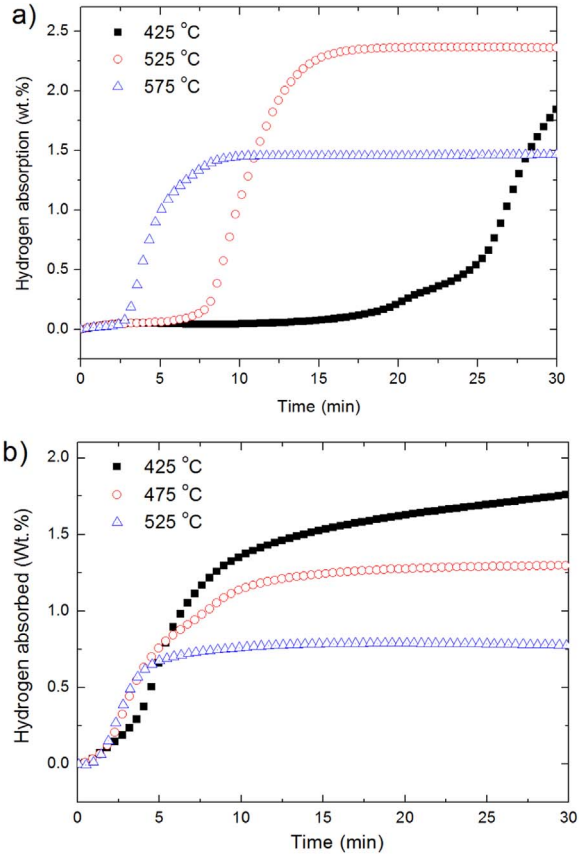

Fig. 4. Hydrogenation in Ar+10%H_2 after cycling in gas containing CO: a) $Ti_{0.9}V_{0.1}$, b) $Ti_{0.9}V_{0.1}$+nano Pd/Pt.

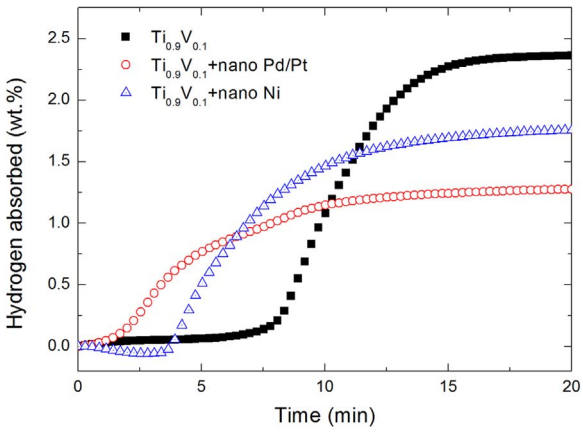

Fig. 5. Hydrogenation curves of $Ti_{0.9}V_{0.1}$ and nanoparticle-deposited $Ti_{0.9}V_{0.1}$ at 475 °C (cycle 6).

incubation time was the shortest after deposition with Pd/Pt nanoparticles. However, a slower hydrogenation kinetics was observed for the particle deposited samples. The Pd/Pt deposited sample had a faster kinetics of the two. It is worth mentioning that the added weight of the particles does not explain the reduced hydrogen capacity of the deposited samples.

As presented above, Pd surprisingly does not improve the tolerance towards CO. For Pd-deposited samples, the amount of hydrogen absorbed during the hydrogenation in gases containing CO was small. The reason for this might be related to the data of the MS study. As can be seen from Fig. 6, the methane formation during the absorption step was quite significant, above 100 ppm, and it increased as the hydrogenation temperature increased. As the methanization involves hydro-

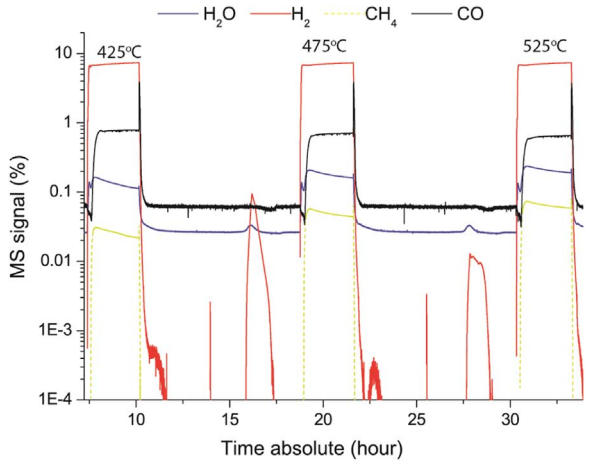

Fig. 6. MS signal during hydrogenation cycle of $Ti_{0.9}V_{0.1}$+nano Pd at 425 °C, 475 °C and 525 °C in Ar+10%H_2+1%CO. The amount of methane was significant and increased upon increasing the hydrogenation temperature.

gen, much hydrogen is consumed during the process. It is worth mentioning that methanization also occurred during the hydrogenation of three types of the alloys, including non-deposited, and Ni- and Pd/Pt deposited samples, but the level of methane formation was below 100 ppm in average.

Fig. 7 shows hydrogen desorption spectra from all dehydrogenation cycles. Hydrogen desorption spectra of non-deposited $Ti_{0.9}V_{0.1}$ are shown in Fig. 7a, and it can be seen that only small amounts of hydrogen were desorbed during cycles 2–4. The hydrogen desorption spectra from cycles 5–7 are composed of one main peak, which is related to the hydrogen desorption from BCC β hydride. Compared to the desorption spectra obtained after the hydrogenation in Ar+H_2 (Fig. 2), the onset temperature for hydrogen desorption was higher, which indicates a formation of the surface layer acting as a barrier for the hydrogenation.

The effect of Pd/Pt nanoparticles on the hydrogen desorption spectrum profiles can be seen in Fig. 7b where the onset temperatures of hydrogen desorption are higher than in Fig. 2 for non-deposited $Ti_{0.9}V_{0.1}$ hydrogenated in Ar+H_2. Again, the reason for this must be in different surface conditions where the nanoparticles play a role. The most important feature that can be observed in Fig. 7b, is that the onset temperatures for hydrogen desorption during the cycles 2–4 are similar to those during the cycles 5–7. This indicates that the nanoparticles had similar effect during hydrogen absorption/desorption independent of CO being present in the gas flow. The effect of Ni was more pronounced than that of Pd/Pt. It can be seen from Fig. 7c that for the Ni-deposited sample, the onset temperature for hydrogen desorption increases very little during the 1st cycle as compared to what was the case for the Pd/Pt-and the non-deposited samples.

After the last cycle, the dehydrogenated alloys were examined by using SEM and XRD. Fig. 8 shows powder diffraction pattern from non-deposited sample and from the samples deposited with Pd/Pt and Ni nanoparticles. It can be seen from the figure that all of the dehydrogenated alloys were composed of an HCP α phase, and that the lattice unit cell parameters of these were almost identical. Only a small amount of the BCC phase was observed and only in the non-deposited sample. This situation is quite different from the hydrogenation of the samples in pure H_2 and dehydrogenation in vacuum, after which almost equal amounts of BCC and HCP phases were formed [10].

Another important point that can be observed in Fig. 8a, is the broadening of the HCP α peak for the non-deposited $Ti_{0.9}V_{0.1}$. This broadening indicates that non-deposited alloy sample has a smaller crystallite size than the samples with nanoparticle deposition. The surface morphology of the dehydrogenated samples without and with nanoparticle (Ni) deposition is shown in the SEM images of Fig. 8b and

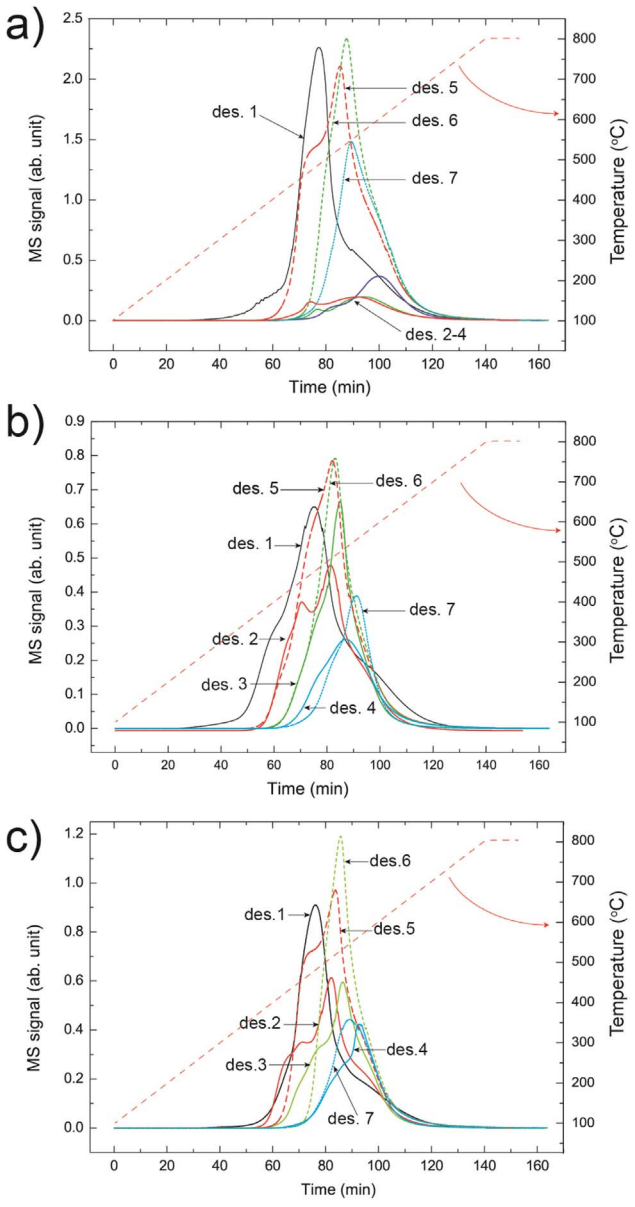

Fig. 7. Hydrogen desorption spectra during non-isothermal heating at 5 K/min from RT to 800 °C of the initial hydride sample (des1), after hydrogenated in Ar+10%H_2+1%CO at 425 °C (des 2), 475 °C (des 3), 525 °C (des 4), and after hydrogenated in Ar+10%H_2 at 425 °C (des 5), 475 °C (des 6), 525 °C (des 7): a) $Ti_{0.9}V_{0.1}$, b) $Ti_{0.9}V_{0.1}$ +nano Pd/Pt, c) $Ti_{0.9}V_{0.1}$+nano Ni.

c. In accordance with the peak broadening observed in Fig. 8a, the non-deposited sample seems to have a finer morphology than the deposited sample. This is also in agreement with the observations of the hydrogenation and dehydrogenation kinetics. From Fig. 5 it seems that the kinetics of hydrogen absorption was faster in the non-deposited sample even though the incubation time was longer, which is explained by smaller crystallite size, which increased the rate of hydrogenation.

3.3. Discussion on the role of nanoparticles

As mentioned earlier, the non-deposited samples absorbed only small amounts of hydrogen in gaseous mixture of argon, hydrogen, and 1% CO. The reason for this was probably a surface blocking effect from atomic/polymeric carbon and methane. Previous investigations have shown that, in hydrogen and at high temperature above~300 °C, CO decomposes on the metal surface leading to the carbon deposition and

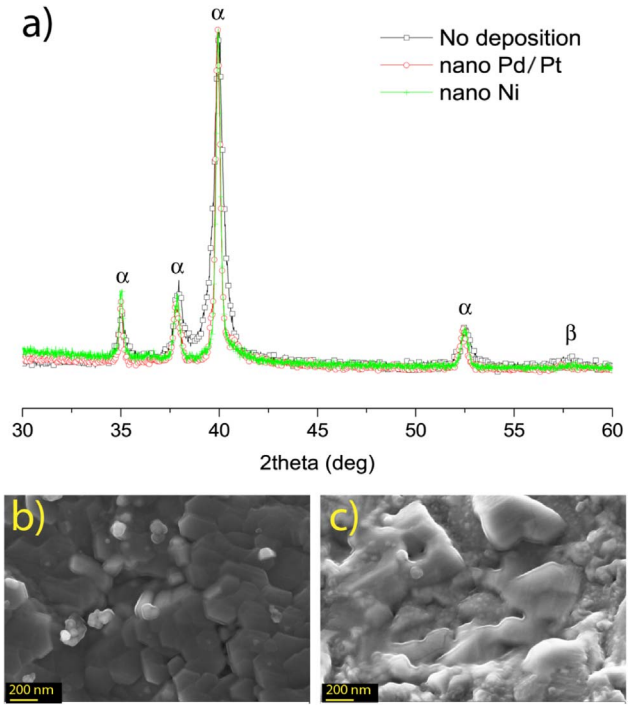

Fig. 8. a) XRD diffraction patterns of the dehydrogenated $Ti_{0.9}V_{0.1}$ alloy after 7 cycles. b) Surface morphology of dehydrogenated non-deposited $Ti_{0.9}V_{0.1}$ alloy, c) Surface morphology of dehydrogenated $Ti_{0.9}V_{0.1}$+nano Ni.

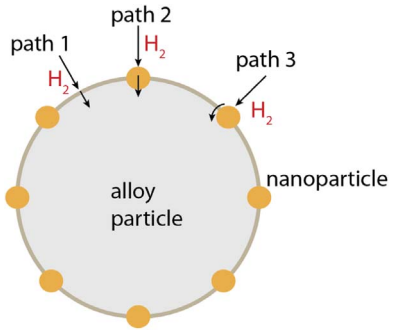

Fig. 9. Model of hydrogen absorption in a nanoparticle-deposited alloy. The sizes of nanoparticle are exaggerated. Path 1: Hydrogen dissociation at the alloy surface providing atomic H; Path 2: Atomic hydrogen is formed during its diffusion through the deposited nanoparticle (Ni; Pd; Pt/Pd); Path 3: Molecular hydrogen dissociates at the interface between the catalyzing nanoparticle and the alloys surface.

methane formation [14]. Atomic and polymeric carbon have been observed to block the hydrogen active sites at the alloy surface so that the hydrogen absorption is inhibited [15–17].

The aims of surface modification are (1) to prevent surface reaction with impure gases, first of all oxidation, (2) to catalyze hydrogen dissociation and absorption, (3) to provide a window for hydrogen absorption with or without any additional catalytic effect [18]. From the results presented above, it can be concluded that the Ni and Pd/Pt nanoparticles have a positive effect on hydrogen absorption by Ti-V alloys in hydrogen gas containing CO. This is in accordance with the results obtained in a previous work by present authors, in which Pd/Pt nanoparticle deposition gave a more positive effect than a deposition of the Pd nanoparticles only [5].

During hydrogen absorption through a nanoparticle deposited metal surface, three absorption paths are possible as illustrated in Fig. 9. If no contaminants are absorbed at the alloy surface, path 1, i.e. H_2 dissociation at the metal surface and diffusion into the metal, is probably the main hydrogen absorption path. If contaminants like C and CO are chemisorbed at the alloy surface, path 2 and 3 are likely to be more efficient, i.e. H_2 dissociates at the nanoparticle surface, and hydrogen diffuses either through the bulk or along the surface layer of the nanoparticle. In path 2, the nanoparticle acts as a window for hydrogen diffusion into the metal. In path 3, hydrogen absorption is caused by a catalytic effect of the nanoparticle and is facilitated by the diffusion of hydrogen at the alloy/nanoparticle interface. In case 2 and 3, hydrogen dissociation at the surface of a nanoparticle is easier because of the breaking of the surface oxide layer. Therefore, the incubation time is eliminated during the hydrogenation of the nanoparticle-deposited alloy. In addition, at a medium temperature, the interface between the nanoparticle and alloy particle is the most efficient diffusion path, so the existence of path 3 facilitates the hydrogenation process.

It is interesting that Ni gave a better effect than Pd/Pt even though it is known that Ni is considered as a methanation catalyst. This could be due to the fact that deposited Ni has an average particle size smaller (~30 nm)than those of Pd/Pt or Pd alone. In fact, Pd, which is known as hydrogenation catalyst, did not give any improvement of the hydrogenation properties of the alloy. The presented MS data shows that there was a significant formation of CH_4 during the hydrogenation of the Pd-deposited samples. The methane formation increased as the temperature increased, and thereby decreased the hydrogenation efficiency. Therefore, the positive effect of the Ni nanoparticles for the hydrogenation of the Ti-V alloys in presense of CO is likely caused by the size effect, further to the catalytic properties of nickel. Further investigation is underway to compare Ni and Pd effect with the same nanoparticle size.

4. Conclusions

The effect of nanoparticle deposition of Ni and Pd and co-deposited Pd/Pt, on hydrogen absorption properties of $Ti_{0.9}V_{0.1}$ has been tested as related to the resistance towards CO gas in the hydrogen-gas mixture. Nanoparticles of Pd (60 nm), Pt/Pd (60 nm) and Ni (30 nm) were deposited using an electroless deposition method. Ni and Pt/Pt nanoparticles improved the resistance of the alloy towards CO while Pd nanoparticles did not give any beneficial effect. The nanoparticles of Ni and Pd/Pt were found to act as catalysts for the hydrogenation and dehydrogenation when the surface of the alloy was contaminated with oxygen or carbon due to chemical transformations of CO. Ni showed a superior performance between all the alternatives.

Acknowledgments

Financial support from the Norwegian Research Council and Statoil ASA are acknowledged.

References

[1] B. Børresen, E. Rytter, I. Aartun, B. Krogh, M. Rønnekleiv, Method and Reactor for Production of Hydrogen. US patent: 20100047158
[2] H. Sakaguchi, T. Tsujimoto, G.-y. Adachi, J. Alloy. Compd. 223 (1995) 122–126.
[3] G.D. Sandrock, P.D. Goodell, J. Less-Common Met. 73 (1980) 161–168.
[4] H. Tanaka, S. Han, Q. Xu, N. Kuriyuma, K. Aihara, N. Taoka, Mater. Sci. Forum (2007) 561–565.
[5] S. Suwarno, Y. Gosselin, J.K. Solberg, J.P. Maehlen, M. Williams, B. Krogh, B.T. Børresen, E. Rytter, E. Ochoa-Fernández, V.A. Yartys, Int. J. Hydrog. Energy 37 (2012) 4127–4138.
[6] M.V. Lototsky, M. Williams, V.A. Yartys, Y.V. Klochko, V.M. Linkov, J. Alloy. Compd. 509 (Supplement 2) (2011) S555–S561.
[7] M. Williams, A.N. Nechaev, M.V. Lototsky, V.A. Yartys, J.K. Solberg, R.V. Denys, C. Pineda, Q. Li, V.M. Linkov, Mater. Chem. Phys. 115 (2009) 136–141.
[8] M. Williams, M. Lototsky, V. Linkov, A. Nechaev, J. Solberg, V. Yartys, Int. J. Energy Res. 33 (2009) 1171–1179.
[9] M. Williams, M.V. Lototsky, M.W. Davids, V. Linkov, V.A. Yartys, J.K. Solberg, J. Alloy. Compd. 509 (Supplement 2) (2011) S770–S774.
[10] S. Suwarno, J.K. Solberg, B. Krogh, S. Raaen, V.A. Yartys, Int. J. Hydrogen Energy 41 (2016) 1699–1710.
[11] S. Suwarno, J.K. Solberg, J.P. Mæhlen, R.V. Denys, B. Krogh, E. Ochoa-Fernández, B.T. Børresen, E. Rytter, I.E. Gabis, V.A. Yartys, Int. J. Hydrogen Energy 38 (2013) 14704–14714.

[12] X.B. Yu, Z. Wu, B.J. Xia, N.X. Xu, J. Alloy. Compd. 386 (2005) 258–260.
[13] S. Suwarno, J.K. Solberg, V.A. Yartys, B. Krogh, J. Alloy. Compd. 509 (Supplement 2) (2011) S775–S778.
[14] C.H. Bartholomew, Appl. Catal. A: Gen. 212 (2001) 17–60.
[15] K. Hou, R. Hughes, J. Membr. Sci. 206 (2002) 119–130.
[16] A. Li, W. Liang, R. Hughes, J. Membr. Sci. 165 (2000) 135–141.
[17] O. Iyoha, B. Howard, B. Morreale, R. Killmeyer, R. Enick, Top. Catal. 49 (2008) 97–107.
[18] X. Shan, J.H. Payer, W.D. Jennings, Int. J. Hydrog. Energy 34 (2009) 363–369.